

# **Joint Statistics of Photon Pathlength and Cloud Optical Depth**

*Q.-L. Min and L. C. Harrison  
Atmospheric Sciences Research Center  
State University of New York  
Albany, New York*

## **Abstract**

A mean pressure- and temperature-weighted photon pathlength in the atmosphere can be inferred from moderate resolution measurements in the O<sub>2</sub> A-band. We show a pathlength retrieval method and calibration results for measurements from a Rotating Shadowband Spectroradiometer (RSS), and present the joint statistics of pathlength and cloud optical depth for cloudy skies observed at the Southern Great Plains (SGP) site from September 30 to December 22, 1997. Two different population branches are apparent in the scattergram of the pathlength versus cloud optical depth; we attribute these to 1) single-layer cases exhibiting small variations of pathlength enhancement over large optical depth ranges; and 2) multiple layer cases with large variances of enhanced photon pathlengths.

## **Introduction**

Remote sensing methods using moderate-resolution O<sub>2</sub> A-band spectroscopy enable retrievals of atmospheric surface pressure and cloud top heights from satellite measurements (O'Brien and Mitchell 1991). These applications are equivalent to the determination of a mean pathlength. With high-resolution spectroscopy, more information about a pathlength distribution can be retrieved (Harrison and Min 1997), but instrumentation requirements are challenging. Pfeilsticker et al. (1998) and Veitel et al. (1998) have recently performed measurements of this kind. We discuss here the utility of moderate resolution spectroscopy; to obtain both mean pathlength and cloud optical depth, for the study of cloud properties.

The RSS is a charge-coupled device (CCD) array spectrograph coupled to an irradiance fore-optic described by Harrison et al. (1998). It uses an automated shadowbanding technique to provide spectrally-resolved direct-normal, diffuse-horizontal, and total-horizontal irradiances, where the passbands and responsivities are guaranteed to be identical for the separated spectral irradiance components. For our purposes, the measurements of the direct solar beam under clear skies then allow accurate calibration of a retrieval for the mean photon pathlength from the oxygen A-band spectroscopy. Once calibrated, the retrieval can be applied to cloudy-sky cases. All results shown here are from the first-generation RSS deployed at the SGP site; its resolution around the Oxygen A-band is  $\approx 9$  nm full-width half-maximum (FWHM), with 2.5 pixels per FWHM. (The second-generation instrument recently deployed has triple the resolution, but as will be discussed this increment in resolution does not permit more pathlength information to be retrieved.)

## Retrieval Algorithm

Absorption by trace gases depends on the photon pathlength distribution. In the case where the radiation arrives from multiple paths the Bouguer-Lambert-Beer law can be rewritten as (Van de Hulst 1980).

$$\frac{I(\lambda)}{I_0(\lambda)} = \int_0^{\infty} e^{-X(\lambda)l} P(l)dl \quad (1)$$

with  $I(\lambda)$  being the irradiance at a wavelength  $\lambda$ ,  $I_0(\lambda)$  the extraterrestrial irradiance,  $X(\lambda)$  the product of cross-section times absorber density,  $l$  the atmospheric pathlength, and  $P(l)$  the pathlength probability distribution function.

For the collision broadening (the dominant broadening mechanism in the lower atmosphere), the shapes of oxygen A-band are assumed to be Lorentzian,

$$k_i = \frac{S_i}{\pi} \frac{\alpha_i}{(v - v_i)^2 + \alpha_i^2} \quad (2)$$

where

$$\alpha_i = \alpha_i^0 \frac{p}{p_0} \left( \frac{T_0}{T} \right)^{1/2} \quad (3)$$

$S$  is the line intensity,  $v$  is the line-center wave number, and  $\alpha_i$  is the linewidth for the  $i$ th line.  $T_0$  and  $p_0$  are standard temperature and pressure respectively. The line intensity  $S$  depends indirectly on temperature due to the populations of the quantum states

$$S = S(T_0) \frac{T_0}{T} \exp\left[1.439E'' \left(\frac{1}{T_0} - \frac{1}{T}\right)\right] \quad (4)$$

where  $E''$  is the energy of the lower state of the transition, which increases significantly from the band center toward the wing region while the normalized line strengths,  $S(T_0)$ , decrease. Thus the line strengths in the wing region are weak, but depend strongly on temperature.

With high-resolution measurements ( $\approx 0.1 \text{ cm}^{-1}$ ) more than one moment of  $P(l)$  can be retrieved (Harrison and Min 1997). However, given the modest resolution of the RSS, where individual lines of the oxygen A-band cannot be resolved, we can retrieve only a mean of a particular moment of the geometric path distribution: that which stems from Eq. (3), the first moment with respect to pressure and the  $-1/2$  moment with respect to temperature. This moment-weighted mean pathlength is naturally expressed in standard airmasses.

Neglecting small variations in oxygen mixing fraction, the oxygen column along the direct-beam path is determined solar zenith angle and surface pressure. To model the direct-beam spectrum we also need the temperature and pressure profile obtained from balloon soundings. In Figure 1, we show the ratios of the measured direct-beam transmissions for five pixels in the RSS spectrum from outside the A-band (topmost) to the band center (bottom), compared to calculations using MODTRAN 3.7 (Berk et al. 1989), then convolved to instrument resolution using laboratory slit-function measurements. The results are very sensitive to both band-model and instrument slit-function; given this, the agreement is good.

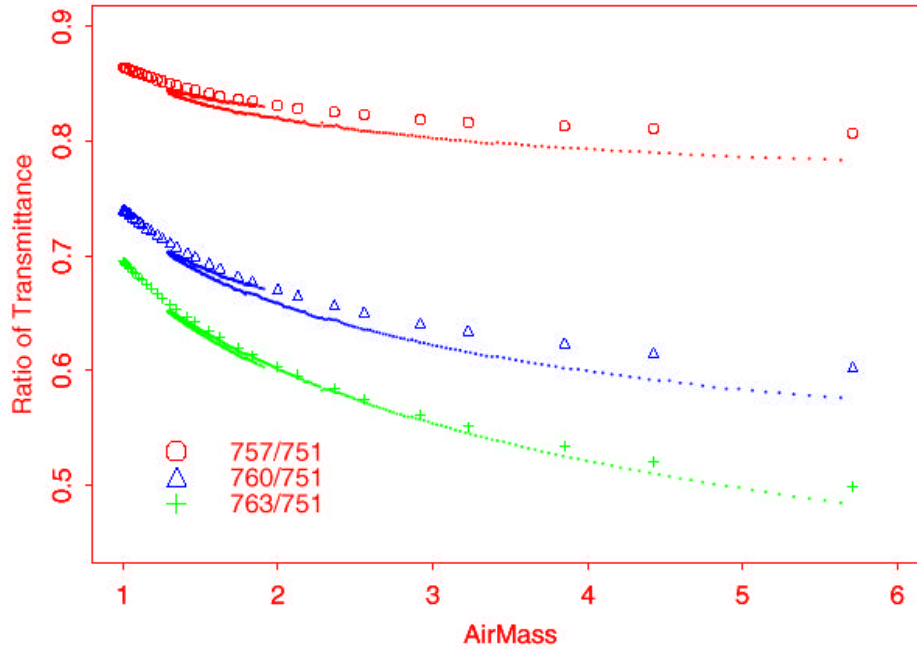


**Figure 1.** Direct-beam transmission for three pixels near 762 nm.

Alternatively, the direct-beam spectra can be used to establish an empirical data set for retrievals under cloudy conditions. To avoid the uncertainties associated with absolute calibrations, we selected a pixel in the RSS spectrum from outside the oxygen A-band (near 751 nm) as a denominator and take the ratios to the pixels inside the A-band.

$$\frac{I(\lambda_i)}{I(\lambda_o)} = \frac{I_o(\lambda_i)}{I_o(\lambda_o)} \int_0^\infty e^{-x(\gamma) \cdot l} P(l) dl \approx \frac{I_o(\lambda_i)}{I_o(\lambda_o)} e^{-f_i(\langle l \rangle)} \quad (5)$$

Where  $f(\langle l \rangle)$  is a function of mean pathlength,  $\langle l \rangle$ . A radiometric transmittance function  $f$  for each specific pixel pair can be fitted from clear-sky direct-beam measurements and then used to obtain the mean pathlength from scattering atmospheres because at the limits of strong- and weak-line approximations, the spectral transmittance can be written by a simple exponential function in terms of the generalized absorption coefficient as (Liou 1992).

$$T(\langle l \rangle) \simeq \begin{cases} \exp(-a \langle l \rangle), & \text{weak line} \\ \exp(-b \sqrt{\langle l \rangle}), & \text{strong line} \end{cases} \quad (6)$$

The measurements from each pixel are convolved across the oxygen A-band, which for terrestrial measurements is always dominated by saturated lines. Nonetheless, to be general we construct the transmittance model for each pixel as a combination of the strong- and weak-line approximation formulae.

In field use the first-generation RSS exhibits wavelength shifts of  $\approx 0.05$  pixel caused by the temperature dependence of the refractive index of the SiO<sub>2</sub> prisms, and the residual variations in temperature ( $< 0.1$  °C) around the instrument's internal thermostatic control point. For most uses of the data, these shifts are negligible, but the A-band retrievals are moderately sensitive to them. Instrument temperatures are monitored in operation; therefore, we use an empirically calibrated transmittance model for each pixel based on the temperature near the detector,  $T_d$ , to account for the wavelength drifting effects:

$$\frac{I(\lambda_i)}{I(\lambda_o)} = \frac{I_o(\lambda_o)}{I_o(\lambda_i)} e^{-(a_1 T_d + a_2) \langle l \rangle^3 - (a_4 T_d + a_5) \langle l \rangle} \quad (7)$$

The  $a_i$  coefficients are determined in the least squares sense to minimize the difference between the transmittance model and observed clear-sky direct-beam ratios. As discussed previously, diffuse-horizontal and direct-normal components share the same instrument optical path. Once the transmittance model for each pixel is developed based on direct beam measurements, we can use it for a retrieval model for the diffuse irradiance to infer the mean photon pathlength in scattering atmospheres.

Figure 2 shows our transmittance model against the clear-sky direct beam observations on December 4, 1997. The two branches, which separate at higher airmass, are the morning and afternoon, due to small differences in internal instrument temperature driven by the warming of the ambient air through the day. This figure also illustrates the sensitivities of the ratios to the pathlength.

## Two Extreme Cases

Before presenting the aggregate data from the SGP site, we show two interesting cases to demonstrate the observing power of these retrievals. Cloud optical depths and mean droplet radii can be obtained from either Multi-Filter Rotating Shadowband Radiometer (MFRSR) or RSS data, and a Microwave Radiometer (Min and Harrison 1996). In all following results optical depths  $< 5$  are determined from the direct-beam extinction. Above five, the optical depth retrieval is that described by Min and Harrison (1996), which uses the total horizontal transmittance at 415 nm and total liquid water column measured by a Microwave Radiometer. This retrieval also yields a mean effective droplet radius. The mean pathlength retrieved from the RSS has been averaged over five-minute intervals to be consistent with the retrievals of cloud optical depth and mean effective radius.

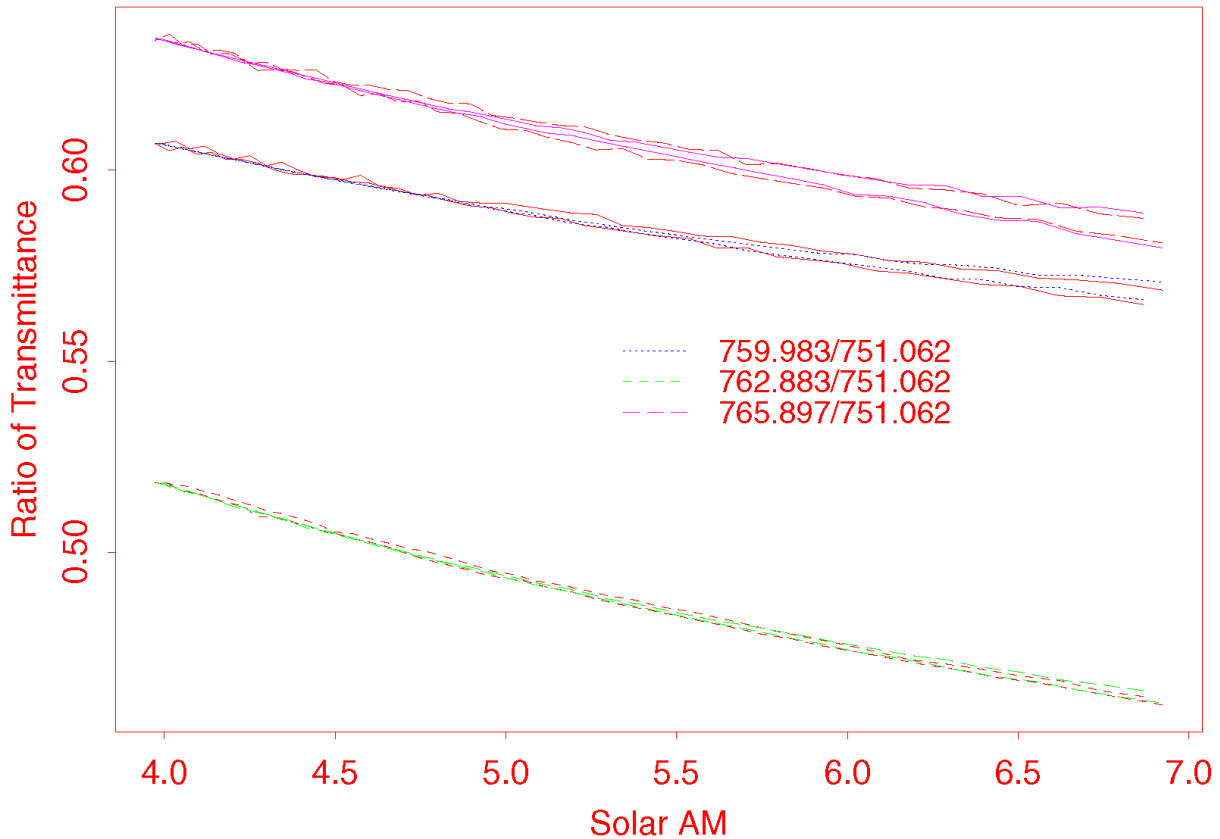


**Figure 2.** Measured and fitted transmittance ratios.

The top panel in Figure 3 shows the time series of mean photon pathlength and cloud optical depth on a day at the SGP site where a stratus overcast continued through the day with variable cloud optical depth. In the bottom panel, the pathlength is shown in two ways as a scattergram versus the cloud optical depth. In the case of this low-level cloud, the photons transit nearly one solar air mass before encountering it; the solid points show the total pathlength minus the direct-beam pathlength: the incremental pathlength due to the cloud. This example is illustrative of many single-layer cloud cases where the pathlength scales linearly with optical depth (in this case over the range 20 to 64) thus exhibiting the Brownian diffusion limit for fixed physical depth. From soundings at the site we believe this is the correct attribution for this stratiform case; however, in general the physical depth of the cloud, or altitude (important because the retrieval is pressure-weighted), may have correlations with optical depth that would alter the apparent slope.

The top panel in Figure 4 shows the time series of mean photon pathlength and cloud optical depth on a day where the pathlength shows much greater variance. Note that this variance is large even for the optical depth  $> 50$  measurements, that occur only after 18:00 Universal Time Coordinates (UTC), where by eye the two seem strongly correlated at the scale of the top panel. Our attribution of the atmospheric state is not certain; we believe this case has a thin and varying upper layer cloud over low stratus. The large pathlength variations then occur due to multiple transits between the layers in cloud-free air that does not contribute to the cloud optical depth.

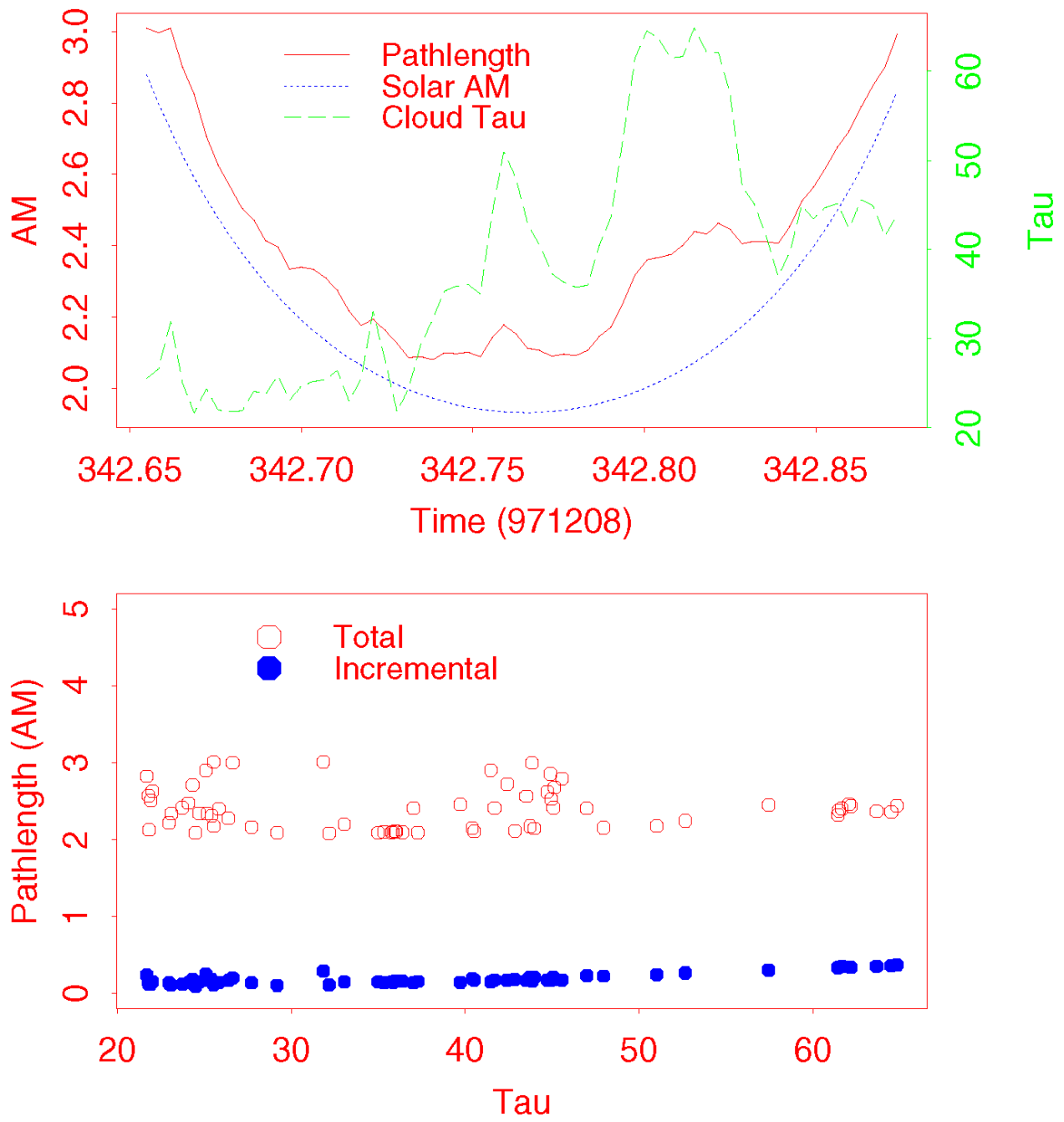


Figure 3. The case of December 8, 1997, at ARM SGP site: The diffusion limit.

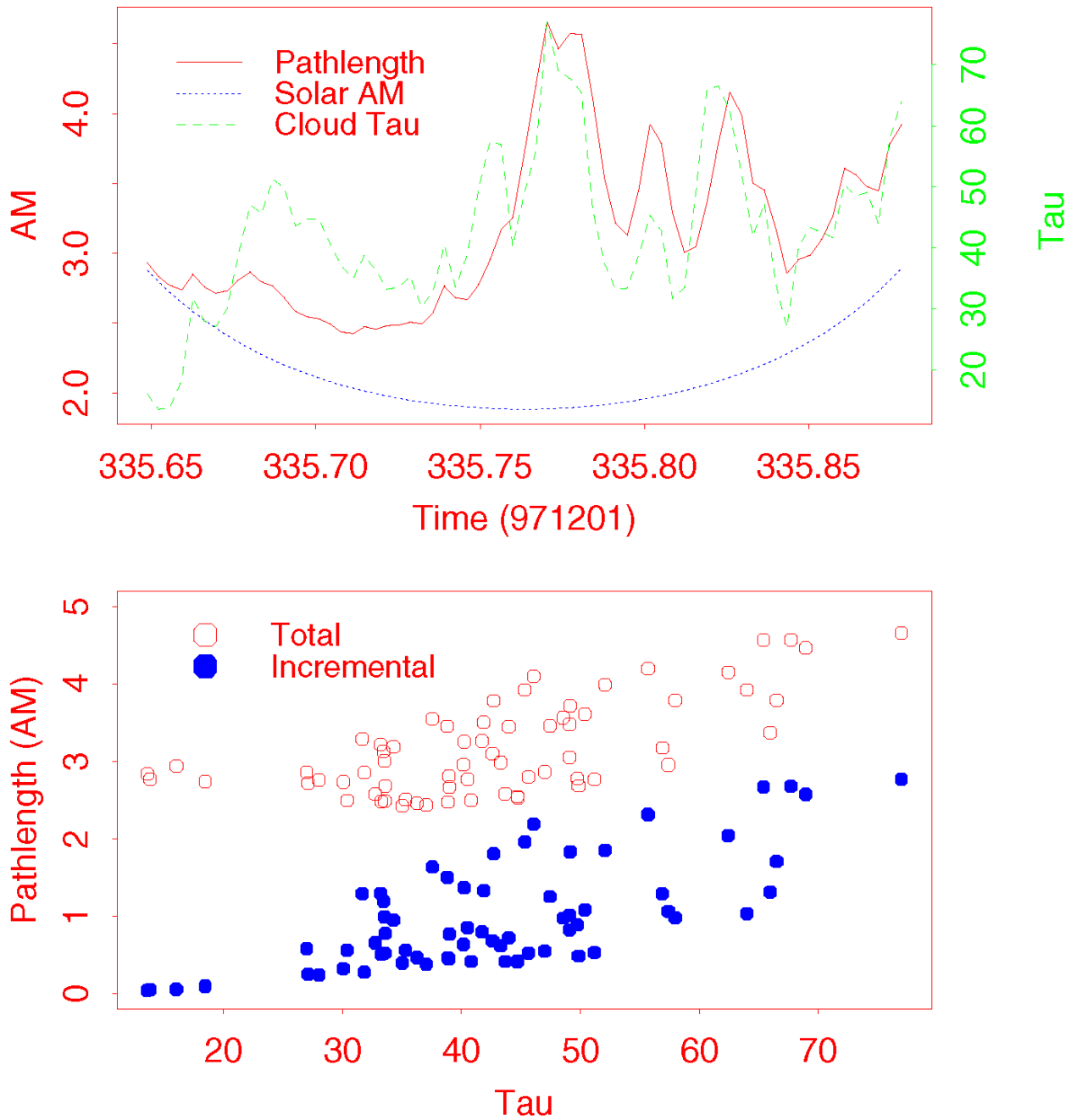


Figure 4. The case of December 1, 1997, at ARM SGP site: A weak upper-layer cloud?

## **Aggregate Statistics**

In the top panel of Figure 5 the incremental-pathlength (= total  $\tau$ -Solar) is plotted as a function of solar airmass for all the data taken at SGP at solar zenith angles  $< 70^\circ$ . The data are segregated into two categories by coincident optical depths with a threshold at optical depth 5. The  $\tau < 5$  distribution appears to bifurcate as the solar airmass increases, with the lower branch exhibiting negative incremental-pathlengths for the greater solar airmasses. Negative incremental pathlengths are possible at larger solar zenith angles due to the pressure weighting; scattering aloft can direct more of the photons vertically downward through the lower atmosphere. Consequently, we believe that the lower branch is caused by thin clouds aloft and the upper branch by low-level aerosols. We plan further work correlating these statistics with lidar measurements to settle this issue.

The lower panel shows incremental-pathlengths versus optical depth. Here we believe that the lowest branch of the data identifies single-layer stratus. Within this population the correlation of mean pathlength and optical depth is driven only in part by the Brownian diffusion scaling expected; the remainder is due to climatological correlation's of stratus altitudes and depths with cloud optical depths at this site.

The scatter of points above this are layered or complex cloud scenes. This joint retrieval permits sensitive detection of structured cloud scenes that might otherwise not be identified. Note the few points with large incremental- pathlengths but low optical depths; when the direct beam can be seen the optical depth is computed from it, but the pathlengths shown here are always for the diffuse-sky component. These are simply cases where the direct beam is momentarily visible through broken cloud layer(s).

## **Discussion**

The mean photon pathlength, together with the cloud optical depth and mean effective droplet radius, describe the optical properties of a warm cloud system and provide strong constraints on geometric properties that may otherwise be unknown. We have shown here that useful information can be obtained with moderate optical resolution: one that is continuously operational so that climatological statistics can be acquired.

For individual cases these allow some classification of cloud and sky scenes that cannot be readily done by other passive remote sensing techniques, particularly the identification of cases where cloud layering or complex structure is producing large photon pathlengths. Further work correlating lidar and cloud radar observations with mean pathlength and optical depth data may strengthen our confidence in the other attributions suggested tentatively here, or suggest new ones.

The climatology of these cloud properties can be used to test the representativeness of general circulation model (GCM) cloud-diagnostic schemes. For any geometrical description of cloud layering and occurrence the optical depth and mean pathlength can be computed, and then compared to observed distributions.

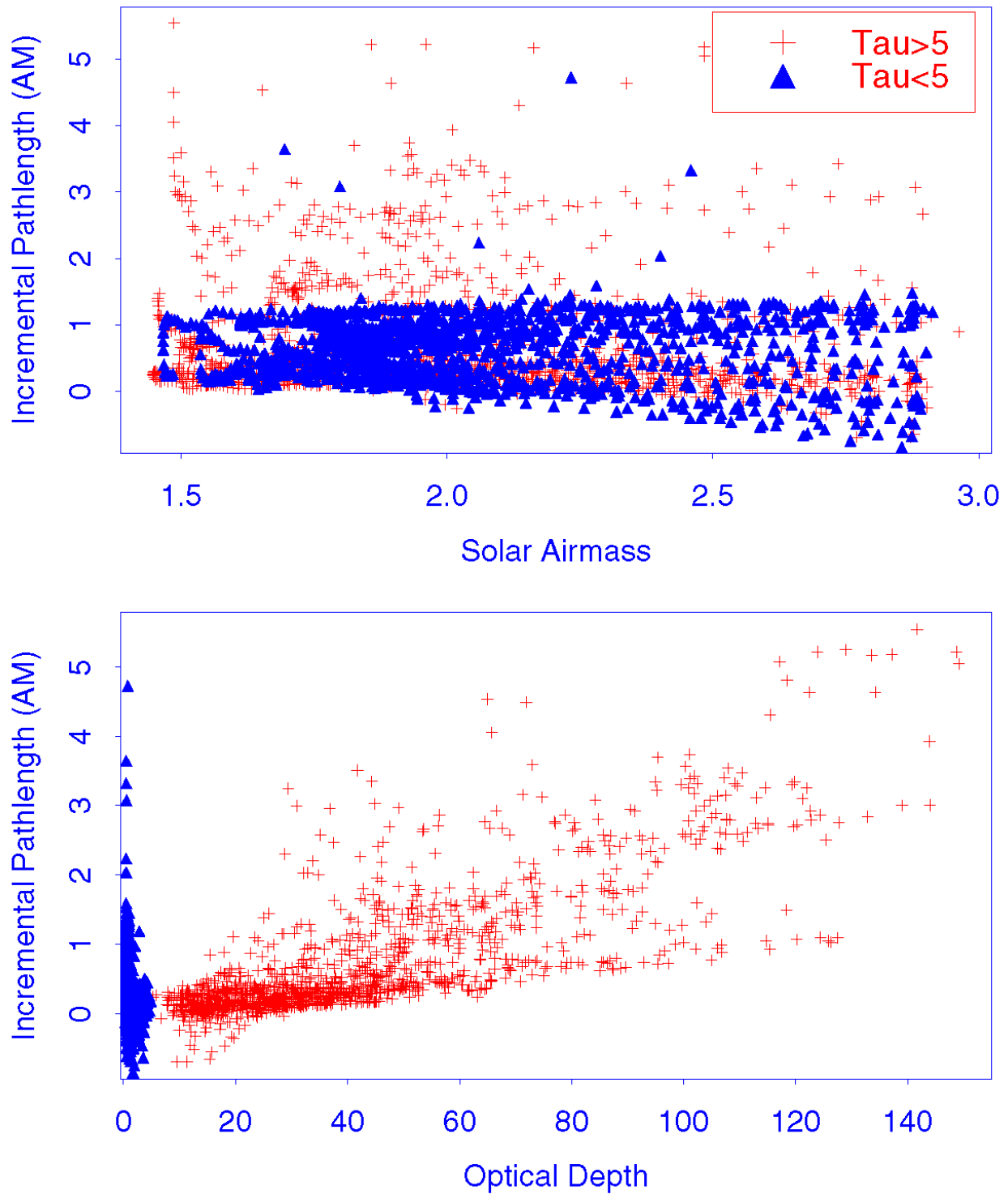


**Figure 5.** Joint statistics of optical depth and photon pathlength: From September 30 to December 22, 1997.

## Acknowledgments

This work was supported by the U.S. Department of Energy Grant DE-FG02-90ER61072 as part of the Atmospheric Radiation Measurement (ARM) Program, and U.S. Department of Agriculture Grant CREES 96-34263-3527 through subcontract G-1421-1.

## References

Berk, A., L. S. Bernstein, and D. C. Robertson, 1989: MOD-TRAN: A moderate resolution model for LOWTRAN7, Report AFGL-TR-89-0122, (Air Force Geophysics Laboratory), Hanscom, Air Force Base, Massachusetts.

Harrison, L., and Q.-L. Min, 1997: Photon pathlength distributions in cloudy atmospheres from ground-based high-resolution O<sub>2</sub> A-band spectroscopy, in IRS'96: Current Problems in Atmospheric Radiation, Eds. W. L. Smith and K. Stamnes. Deepak Publ., Hampton.

Harrison, L. C., M. Beauharnois, J. Berndt, P. Kierdron, J. Michalsky, Q.-L. Min, 1998: The Rotating Shadowband Spectroradiometer (RSS) at the Southern Great Plains (SGP). *Geophys. Res. Lett.* Submitted.

Liou, K.-N., 1992: Radiation and cloud processes in the atmosphere. Oxford Univ. Press, New York.

Min, Q.-L., and L. C. Harrison, 1996: Cloud properties derived from surface MFRSR measurements and comparison with GEOS results at the ARM SGP site. *Geophys. Res. Lett.*, **23**, 1641.

O'Brien, D. M., and R. M. Mitchell, 1991: Error estimates for retrieval of cloud top pressure using absorption in the A-band of oxygen. *J. Appl. Meteor.*, **31**, 1179.

Pfeilsticker, K., F. Erle, H. Veitel, and U. Platt, 1998: First geometrical pathlengths probability density function derivation of the skylight from spectroscopically highly resolving oxygen A-band observations 1. Measurement technique, atmospheric observations, and model calculations. *J. Geophys. Res.*, **103**, 11,483.

Van de Hulst, H. C., 1980: Multiple light scattering. Academic Press, New York.

Veitel, H., O. Funk, C. Kruz, U. Platt, and K. Pfeilsticker, 1998: Geometrical path length probability density functions of the skylight transmitted by midlatitude cloudy skies: Some case studies. *Geophys. Res. Lett.*, **25**, 3355.